

To be submitted to: Nucl. Phys A.

The $\pi\pi$ interaction in nuclear matter from a study of the $\pi^+A \rightarrow \pi^+\pi^\pm A'$ reactions

F. Bonutti^{a,b}, P. Camerini^{a,b}, E. Fragiaco^{a,b}, N. Grion^{a,1}, R. Rui^{a,b}, J.T. Brack^{c,2}, L. Felawka^c, E.F. Gibson^f, G. Hofman^{d,2}, M. Kermani^d, E.L. Mathie^e, R. Meier^{c,3}, D. Ottewell^c, K. Raywood^c, M.E. Sevier^g, G.R. Smith^c and R. Tacik^e.

^a *Istituto Nazionale di Fisica Nucleare, 34127 Trieste, Italy*

^b *Dipartimento di Fisica dell'Universita' di Trieste, 34127 Trieste, Italy*

^c *TRIUMF, Vancouver, B.C., Canada V6T 2A3*

^d *Department of Physics and Astronomy, University of British Columbia, Vancouver, B.C., Canada V6T 2A6*

^e *University of Regina, Regina, Saskatchewan, Canada S4S 0A2*

^f *California State University, Sacramento CA 95819, USA*

^g *School of Physics, University of Melbourne, Parkville, Vic., 3052, Australia*

The CHAOS Collaboration

The pion-production reactions $\pi^+A \rightarrow \pi^+\pi^\pm A'$ were studied on 2H , ^{12}C , ^{40}Ca , and ^{208}Pb nuclei at an incident pion energy of $T_{\pi^+}=283$ MeV. Pions were detected in coincidence using the CHAOS spectrometer. The experimental results are reduced to differential cross sections and compared to both theoretical predictions and the reaction phase space. The composite ratio $\mathcal{C}_{\pi\pi}^A$ between the $\pi^+\pi^\pm$ invariant masses on nuclei and on the nucleon is also presented. Near the $2m_\pi$ threshold pion pairs couple to $(\pi\pi)_{I=J=0}$ when produced in the $\pi^+ \rightarrow \pi^+\pi^-$ reaction channel. There is a marked near-threshold enhancement of $\mathcal{C}_{\pi^+\pi^-}^A$ which is consistent with theoretical predictions addressing the partial restoration of chiral symmetry in nuclear matter. Furthermore, the behaviour of $\mathcal{C}_{\pi^+\pi^-}^A$ is well described when the restoration of chiral symmetry is combined with standard P-wave renormalization of pions in nuclear matter. On the other hand, nuclear matter only weakly influences $\mathcal{C}_{\pi^+\pi^+}^A$, which displays a flat behaviour throughout the energy range regardless of A .

PACS:25.80 Hp

¹Corresponding author, electronic mail: Nevio.Grion@ts.INFN.it

²Present address: University of Colorado, Boulder CO 80309-0446, USA

³Permanent address: Physikalisches Institut, Universität Tübingen, 72076 Tübingen, Germany

1. Introduction

The influence of the nuclear medium on the $\pi\pi$ interaction was investigated at TRIUMF using the pion induced pion-production reactions $\pi^+A \rightarrow \pi^+\pi^\pm A'$ (henceforth labelled $\pi 2\pi$). The initial study was directed to the reactions in deuterium, that is, to $\pi^+n(p) \rightarrow \pi^+\pi^-p(p)$ and $\pi^+p(n) \rightarrow \pi^+\pi^+n(n)$, in order to understand the $\pi 2\pi$ behaviour on both a neutron and a proton through quasi-free reactions. The $\pi 2\pi$ process was then examined on the complex nuclei ^{12}C , ^{40}Ca and ^{208}Pb in order to study possible $\pi\pi$ medium modifications by direct comparison of the $\pi 2\pi$ data. To ensure the validity of this approach, the following experimental method was applied. All the $\pi 2\pi$ data were taken under the same kinematical conditions. The final $\pi^+\pi^\pm$ pairs were detected in coincidence to ensure a reliable identification of $\pi 2\pi$ events. Pion pairs were analysed down to 0° $\pi\pi$ opening angles to determine the $\pi\pi$ invariant mass at the $2m_\pi$ threshold. The energy of the incident pion beam, $T_{\pi^+}=283$ MeV, was chosen to enable the investigation of the $\pi A \rightarrow \pi\pi A'$ reaction in the near-threshold region.

In early experimental works on $\pi 2\pi$ in nuclei it was observed that (i) pions preferentially populate the low-energy part of the kinetic energy spectra [1, 2, 3], and (ii) the $\pi^+\pi^-$ invariant mass $M_{\pi^+\pi^-}^A$ peaks increasingly toward the $2m_\pi$ threshold as the nucleus mass number increases [3]. The property (i) could not be explained in terms of the $\pi^+A \rightarrow \pi^+\pi^-p[A-1]$ phase space [1]. Nor was a detailed model of the $A(\pi^+, \pi^+\pi^-)$ reaction [4] able to reproduce the low-energy pion yield, although it embodied the kinematical limits of the experimental apparatus. The same model, however, could correctly predict the total cross section of the $\pi 2\pi$ reaction in nuclei [5], as well as many-fold differential cross sections [2]. A novel approach [6] was then employed to explain the near threshold behaviour of $M_{\pi^+\pi^-}^A$, i.e. the property (ii). In this approach a $\pi\pi$ pair is considered as a strongly interacting system when the two pions couple to the $I=J=0$ quantum numbers. The $(\pi\pi)_{I=J=0}$ properties in nuclear matter are studied by dressing the single-pion propagator to account for the P -wave coupling of pions to *particle - hole* and Δ - *hole* configurations. The model is able to explain the general features of the $M_{\pi^+\pi^-}^A$ distributions, which are predicted to increasingly accumulate strength near the $2m_\pi$ threshold for ρ , the nuclear medium density, approaching ρ_0 , the saturation density. However, within the same theoretical framework, the near-threshold strength of the $\pi\pi$ T -matrix is considerably reduced when the $\pi\pi$ interaction is constrained to be chiral symmetric [7]. This may indicate that effects other than the in-medium $(\pi\pi)_{I=J=0}$ interaction contribute to the observed strength. Conversely, the absence of any in-medium modification of the $(\pi\pi)_{I=J=0}$ interaction leads to $M_{\pi^+\pi^-}^A$ distributions which lack of strength at threshold. This is shown in the work of [3], which compares the experimental results with the model predictions of [4].

Some $\pi 2\pi$ articles were recently published by the CHAOS collaboration at TRIUMF. The novel data highlighted some properties of the in-vacuum $\pi\pi$ interaction [8, 9, 10], as well as the in-medium modifications of the $\pi\pi$ interaction [11, 12, 13]. The appearance of the CHAOS results have renewed theoretical interest, which now bases the interpretation of

the $\pi 2\pi$ and $\pi\pi$ data on some common features:

1. The $\pi\pi$ interaction is strongly influenced and modified by the presence of the nuclear medium when the $\pi\pi$ interaction occurs in the $(\pi\pi)_{I=J=0}$ channel, conventionally called the σ -channel [6, 14, 15, 16, 17].
2. Nuclear matter affects the $(\pi\pi)_{I=2,J=0}$ interaction only weakly [16, 18].
3. Models which only include standard many-body correlations, i.e. the P -wave coupling of π' s to $p-h$ and $\Delta-h$ configurations, are able to explain part of the observed $M_{\pi^+\pi^-}^A$ -yield near the $2m_\pi$ threshold [14, 16, 18].

In recent theoretical works on the $(\pi\pi)_{I=J=0}$ interaction in nuclear matter [19], the effects of standard many-body correlations have been combined with those derived from the restoration of chiral symmetry in nuclear matter. The resulting $M_{\pi^+\pi^-}^A$ distributions regain strength near the $2m_\pi$ threshold as A (thus the average ρ) increases. Such behaviour was outlined in some earlier theoretical works, which demonstrated that the $M_{\pi^+\pi^-}^A$ enhancement near threshold is a distinct consequence of the partial restoration of the chiral symmetry at $\rho < \rho_0$ [17]. The purpose of this article is to present a comprehensive set of $\pi 2\pi$ data and to discuss them in the light of the most recent theoretical findings.

Some of the characteristics of the $\pi 2\pi$ process in nuclei were presented in Refs.[1, 2, 3, 5, 8, 11, 12] and some observables, those most sensitive to the $\pi\pi$ interaction, were discussed in Ref.[13]. These TRIUMF results are presented in the form of many-fold differential cross sections, which are of interest in the current work. Most other $\pi 2\pi$ measurements deal only with total cross sections. These include old data taken with emulsion techniques [20], and more recently, with a magnetic spectrometer similar to CHAOS [21]. Since $\pi 2\pi$ total cross sections are not part of the present discussion, these data will not be considered in this work. The article is organised as follows: some features of the experiment are reported in Sec. 2. Sec. 3 deals with the data analysis. The available $\pi 2\pi$ models are presented in Sec. 4. The $\pi 2\pi$ data are discussed in Sec. 5. Other existing results are mentioned in Sec. 6. Finally, conclusions are summarised in Sec. 7.

2. The experiment

The experiment was carried out at the TRIUMF Meson Facility. Incident pions were produced by the collision of 480 MeV protons on a 10 mm thick graphite target. The M11 pion beam line transported the 282.7 MeV pions to the final focus which was located at about 14 m from the production target. M11 was tuned to focus the pion beam on the target, which was placed at the centre of the CHAOS spectrometer. Pion pairs were detected

in coincidence to ensure a unique identification of the pion production process.

2.1 The pion beam, the beam monitor and the beam counting

The M11 pion channel was set to deliver positive pions with a central momentum $p=398.5$ MeV/c. The beam momentum spread ($\Delta p/p$) was defined by slits which were located at the intermediate dispersed focus of the channel. The particle beam was mainly composed of pions and protons, $\pi : p \approx 1 : 10$. The fraction of positive electrons and muons was negligible, typically $\pi : \mu : e = 1.0 : 0.003 : 0.002$ [22]. The proton contamination was moderated by a CH2 absorber placed at the mid-plane of the M11 channel: the energy deposited by protons in the absorber degraded the central momentum of the proton distribution so that most of them were intercepted by the slits of the channel. Pions were finally discriminated from protons with a plastic scintillator counter placed transversally to the particle beam at about 194 cm upstream of the target. The pulse height (PH) associated with the passage of a proton through the plastic scintillator was over 3 times higher than the pulse height of a pion of the same momentum, i.e. $PH_p/PH_\pi \simeq 3$ at 400 MeV/c. This allowed for a fast discrimination between the two beam components and, ultimately, the determination of the beam composition, which was monitored throughout the experiment. The systematic uncertainty in determining the fraction of pion f_π in the particle beam was about 1%.

The beam monitor (M_b) consisted of 4 slabs of Pilot U plastic scintillator 3 mm thick, with a combined cross-sectional area of 9×26 cm². This area was wide enough to contain the full particle beam. Each segment of the monitor was designed to count roughly the same beam flux, i.e. 1.0-1.5 MHz for ¹²C, ⁴⁰Ca and ²⁰⁸Pb targets, and ≤ 0.5 MHz for ²H (see Table 1). The four segments were coupled through lucite light guides to four fast-counting tubes in order to avoid piling-up of the output pulses. The beam monitor was placed at about 161 cm from the CHAOS dipole tip edge to prevent any background arising from the interaction of pions and protons with the monitor medium from entering the spectrometer. However, with such an arrangement of the beam monitor, an appreciable fraction of the pions crossing it decayed before reaching the target. The decay rate was $f_d = 8\%$ and the uncertainty in assessing f_d is negligible. The beam momentum spread ($\Delta p/p$ at FWHM, [%]), total intensity over all segments (N , [10^6 particles/s]) and composition ($\pi : p : \mu : e$) at the monitor location are summarised in Table 1.

The beam monitor was only capable of counting the number of incident particle bursts N_i . Depending on its intensity, a ~ 5 ns FWHM beam burst may have contained one or more particles, i.e. pions and protons. Therefore the effective number of particles traversing the monitor is $N_m = \mu_p N_i$, where μ_p is the average number of particles per beam burst. Since particle counting follows Poisson statistics, the average number of particles is $\mu_p = -\ln(1 - r)/r$, where $r = N_i/N_p$ and N_p is the number of primary proton bursts per second

Table 1: Characteristics of the particle beam at the monitor location: momentum spread ($\Delta p/p$ at FWHM, [%]), intensity (N , [10^6 particles/s]) and composition ($\pi : p : \mu : e$).

Nucleus	$\Delta p/p$	N	$\pi : p : \mu : e$
2H	0.8	1.6	3.2:1.0:0.01:<0.01
${}^{12}C, {}^{40}Ca, {}^{208}Pb$	1.2	4-5	4.3:1.0:0.01:<0.01

23.06×10^6 . In the present measurement the maximum number of particles traversing a monitor single slab did not exceed $1.5 \times 10^6/s$. Thus, the percentage of particles not counted by the monitor was $100(\mu_p - 1) < 3.5\%$, and the uncertainty associated with this correction is negligible.

The number of pions at the target location was finally given by the equation $N_\pi = \mu_p(1 - f_d)f_\pi N$, and the uncertainty in assessing N_π was slightly above 1%.

2.2 The targets

The targets used in this experiment were either solid self-supporting plates of carbon, calcium, and lead, or a vessel for the liquid deuterium. The targets were located at the centre of the dipole, and their characteristics are summarised in Table 2.

The deuterium target consisted of a low-mass cylindrical vessel filled with liquid deuterium. It was continuously cooled by a refrigerator, and then warmed to its operating temperature, which was monitored both by an external helium gas thermometer and direct measurement of the vapour pressure of the deuterium. The variation of density due to the uncertainty in temperature ($23.0 \pm 0.2K$) was negligible. The variation of density due to the formation of bubbles throughout the liquid was larger, and most significant near the top of the target cell. The variation of thickness of the target cell due to bulging outward of the thin windows contributes a further uncertainty to the target thickness. Both of these effects were convoluted with measured beam profiles to determine the areal target thickness. The total number of scattering centres was evaluated by integrating the beam profile over that of the target, which was determined by tracing elastically scattered pions during a calibration run. The uncertainty in the areal target thickness was estimated to be 3%. In order to evaluate the contribution of the background from the target vessel, a dedicated run was performed with the deuterium target emptied. Then, the rejection of events with the reaction vertex on the vessel reduced the background to about 2%. A reconstructed interaction vertex for a vessel of the same dimensions as the one used in the present experiment is shown in Fig. 2 of Ref.[9].

Table 2: Characteristics of the targets used in the experiment.

	2H	${}^{12}C$	${}^{40}Ca$	${}^{208}Pb$
type	liquid in cyl. vessel	solid plate	solid plate	solid plate
thickness	H: 5 cm, ϕ : 5 cm	0.332 g/cm ²	0.180 g/cm ²	0.604 g/cm ²
area	–	$70 \times 61mm^2$	$55 \times 46mm^2$	$74 \times 58mm^2$

The solid targets were made of self-supporting plates surrounded by a frame for handling. The frame was made of lucite for the ${}^{12}C$ and ${}^{208}Pb$ targets, and alluminum for the ${}^{40}Ca$ target. The target thicknesses and areas are listed in Table 2. The areal size of the plates was large enough to entirely contain the beam spot. The beam envelope at the target location was measured previously [23], and was found to be entirely confined to an area of $\sim 40 \times 40mm^2$. This can be seen in Fig. 1, which illustrates the vertex reconstruction

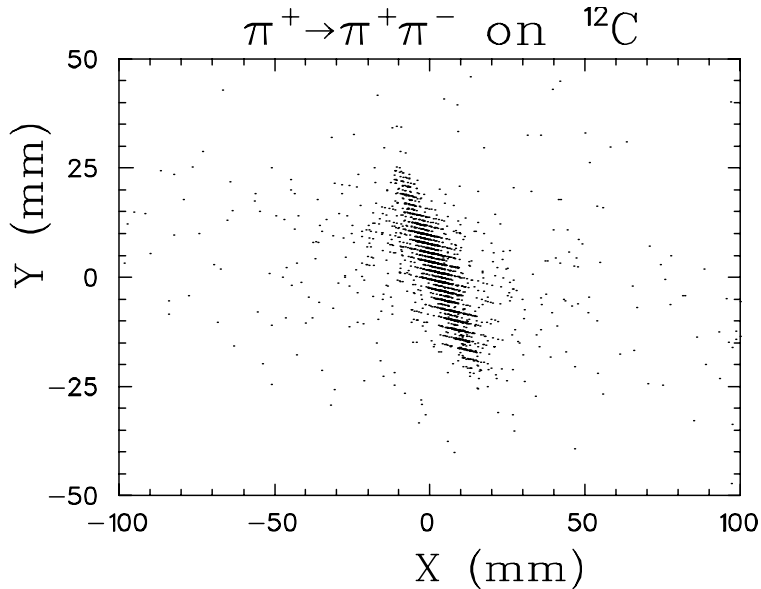


Figure 1: Horizontal beam profile at the ${}^{12}C$ target location. The interaction vertex is reconstructed for $\pi^+ \rightarrow \pi^+\pi^-$ events. The profile full-width of the target about 55 mm is entirely contained in the physical target, which has a width of 70 mm as reported in Table 2.

provided by the CHAOS spectrometer from $\pi^+ \rightarrow \pi^+\pi^-$ events on ${}^{12}C$. Analogous results were obtained for the other solid targets.

2.3 The CHAOS spectrometer and triggering system

CHAOS is a magnetic spectrometer which was designed for the detection of multi-particle

events in the medium-energy range [24]. The magnetic field is generated by a dipole whose pole tip is 66 cm in diameter. The magnet is capable of producing a field intensity up to 1.6 T with an uniformity of about 1%. There is a 12 cm bore at the centre for the insertion of targets. Fig. 2 illustrates a reconstructed $\pi_i^+ \rightarrow \pi^+\pi^-p$ event on ^{12}C , and

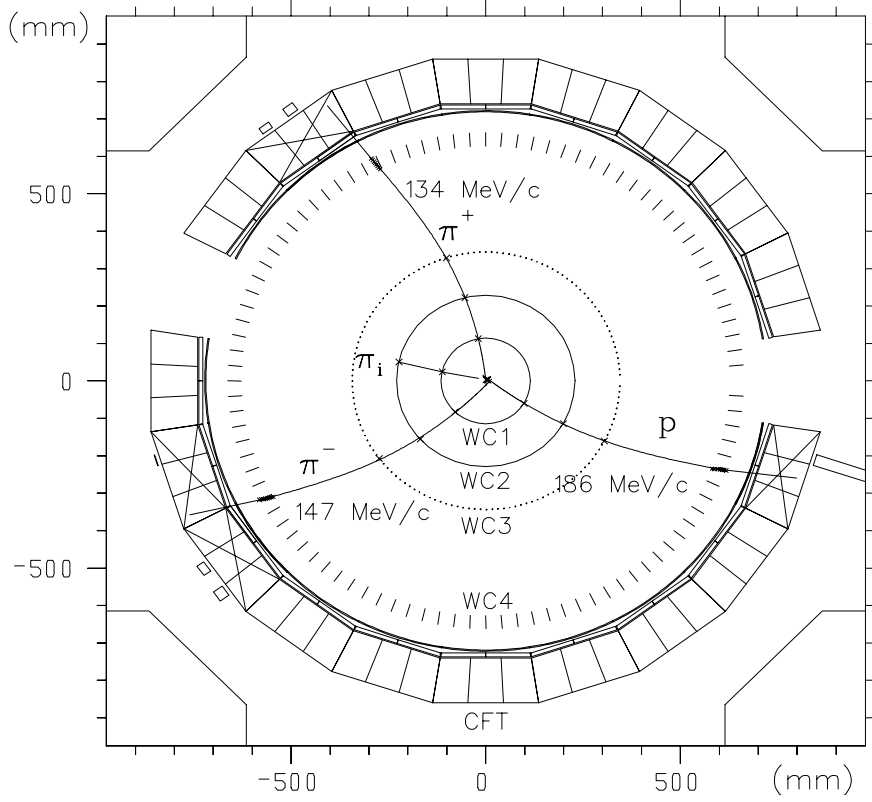


Figure 2: Reconstructed particle trajectories in CHAOS for the $\pi_i^+ \rightarrow \pi^+\pi^-p$ reaction on ^{12}C , the geometrical disposition of the wire chambers (WC), the first level trigger hardware (CFT) and the magnet return yokes in the corners. Two CFT segments are removed to permit the particle beam (π_i) to traverse the spectrometer. The CFT segments which are hit by particles are marked with crosses, and the energy deposited in the first two layers ($\Delta E1$ and $\Delta E2$) is indicated by boxes. The proton has a momentum slightly above the CHAOS threshold (185 MeV/c), and its energy is fully deposited in $\Delta E1$.

shows the geometrical disposition of the wire chambers (WC), the CHAOS first level trigger hardware (CFT), and the magnet return yokes in the corners. WC1 and WC2 are multiwire proportional chambers which are capable of handling rates exceeding 5×10^6 particles/s for extended periods of time with high efficiency ($\sim 95\%$). They are cylindrical in shape, with diameters of 22.8 cm and 45.8 cm, respectively. WC3 is a cylindrical drift chamber designed to operate in a magnetic field [25]. Its diameter is 68.6 cm. The outermost chamber, WC4, is a vector drift chamber 122.6 cm in diameter, which operates in the tail of the magnetic field of CHAOS. The segments of WC3 and WC4 which were crossed by the incident particle beam were turned off. The CFT hardware consists of three adjacent cylindrical layers of fast-counting detectors [26]. The first two layers ($\Delta E1$ and $\Delta E2$) are NE110 plastic scintillators

0.3 cm and 1.2 cm thick, respectively. $\Delta E1$ is 72 cm from the magnet centre and spans a zenithal angle of $\pm 7^\circ$; thus, it defines the geometrical solid angle of CHAOS $\Omega=1.5$ sr. The third layer is a SF5 lead-glass 12.5 cm thick, about 5 radiation lengths, which is used as a Cerenkov counter. The three layers were segmented in order to provide an efficient triggering system for multi-particle events. Each segment covered an azimuthal angle (i.e., in-the-reaction plane) of 18° . During data taking two segments were removed in order to allow the passage of the particle beam (see Fig. 2).

The experiment relied on two on-line triggers: the first ($1^{st}LT$) [26] and second ($2^{nd}LT$) [27] level trigger. The logical signals which were issued by the CFT following $\pi^+ \rightarrow \pi^+\pi^\pm$ events were initially pipe-lined and then filtered by requiring a coincidence $M_b \times (\Delta E1 \times \Delta E2)_i \times (\Delta E1 \times \Delta E2)_j$ with $i, j = 1, \dots, 18$ and $i \neq j$. Such a logic analysis was performed at a rate of about 30 MHz. Despite of the fast filtering, the $1^{st}LT$ trigger was overwhelmed ($>99.99\%$) by multi-particle events from competing reactions: quasi-elastic scattering (qes) $\pi^+ \rightarrow \pi^+p(d)$, and pion absorption (abs) $\pi^+ \rightarrow pp$. This called for a second and more selective triggering system, which was based on the information delivered by the innermost wire chambers. For each event passed by the $1^{st}LT$, the $2^{nd}LT$ trigger calculated the momentum of each track, its polarity and the reaction vertex topology. It then compared a combination of these parameters with predefined criteria. When the criteria were fulfilled the event was accepted and recorded on tape, otherwise a fast clear signal was sent to the readout electronics, and the two triggers were reset. An entire $2^{nd}LT$ cycle was accomplished in $< 10\mu s$, depending on the number of reconstructed tracks. The event rate recorded on tape ranged from 30 to 100 Hz depending on the nucleus studied. Roughly 0.1% of the recorded events were $\pi \rightarrow \pi\pi$ as determined by detailed off-line analysis.

2.4 The CHAOS acceptance and performance

In the present measurement CHAOS was operated with a magnetic field of 0.5 T. The field and the energy deposited by the particles emerging from the target in the WC's and $\Delta E1$ media determined the CHAOS threshold, which was 57 MeV/c for pions. The pion threshold can be observed in Fig. 3, which shows a diffusion plot of the π^\pm momenta (p_π) versus their azimuthal angles (Θ_π), for the $\pi^+ \rightarrow \pi^+\pi^-$ reaction channel on ^{12}C . The figure also depicts the overall CHAOS acceptance for pions. The removal of the two CFT segments intercepting the particle beam defines strips in the (p_π, Θ_π) plane which are unreachable by pions. These strips are confined within bounds (continuous lines), which are the results of GEANT Monte Carlo simulations. The strips are 14° wide, 4° narrower than a CFT segment. The narrowing is due to the circular trajectories that pions acquire by moving in the magnetic field of CHAOS, which ultimately defines the exit direction of pions before impinging upon $\Delta E1$. For both positive and negative pions the removal of the CFT segment which allows the particle beam to enter CHAOS (strip at around 180°) negligibly affects the reaction phase space. The missing CFT segment at the exit (strip at around 0°) somewhat restricts the available $\pi \rightarrow \pi\pi$ phase space. However, the limitation is only for an angular

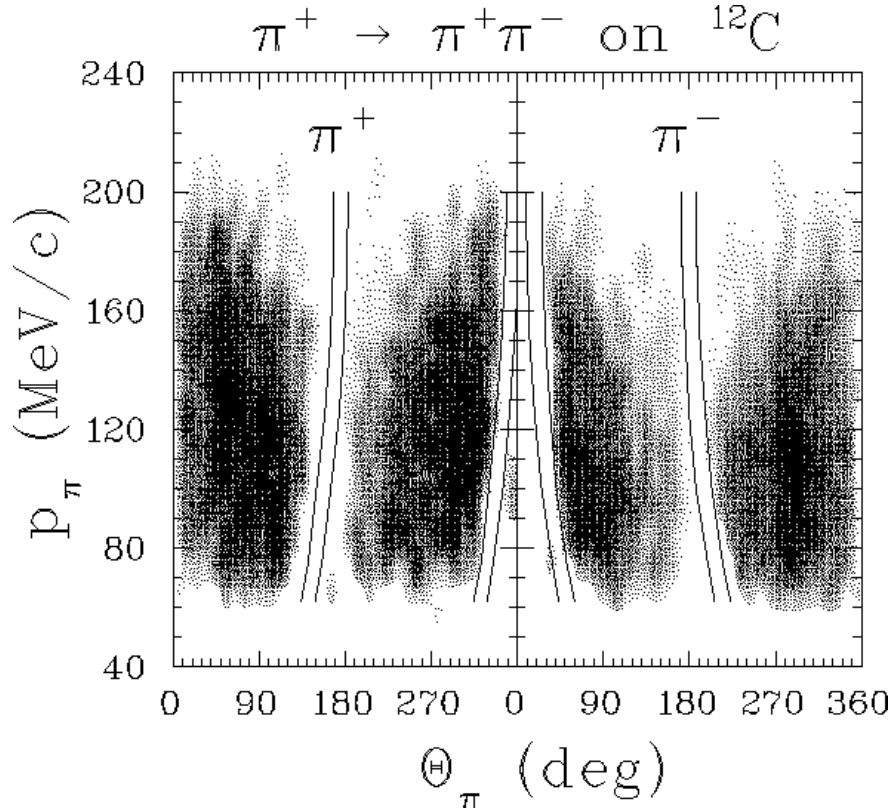


Figure 3: Diffusion plot of the CHAOS acceptance to pions of the $\pi^+ \rightarrow \pi^+\pi^-$ reaction on ^{12}C . The continuous lines confine the (p_π, Θ_π) phase space unreachable by pions, and are the result of GEANT Monte Carlo simulations. The strips are 14° wide.

interval of 14° .

The acceptance of CHAOS is irregular in the (p_π, Θ_π) plane due to the finite segmentation of the CFT, the two missing CFT segments, and the pion decays inside CHAOS. All these sources of non-uniformity were accounted for by assigning a *weight* to each $\pi \rightarrow \pi\pi$ event. The weights were determined using GEANT Monte Carlo simulations, as described in more detail in Ref.[8]. Weight distributions are represented in Fig. 4 for the two $\pi^+ \rightarrow \pi^+\pi^\pm$ reaction channels on ^{12}C . These distributions show a similar behaviour: they are peaked around 1.5 and have a tail which extends up to 8. Since each $\pi\pi$ event was binned with its weight, to avoid large corrections in the distributions, weights were restricted to vary from >0 to $\mu + 2\sigma$, where μ is the mean value and σ is the standard deviation of the weight distribution. For $\pi^+\pi^+$ events, $\mu(\sigma) = 2.43(1.42)$, while for $\pi^+\pi^-$ events, $\mu(\sigma) = 2.52(1.31)$.

As an example, in Fig. 5 are reported the weight distributions used to correct the measured invariant mass spectra for the two $\pi^+ \rightarrow \pi^+\pi^\pm$ reaction channels on ^{12}C . The average uncertainty in the weight is $\sim 6\%$ [8]. The distributions are represented over an

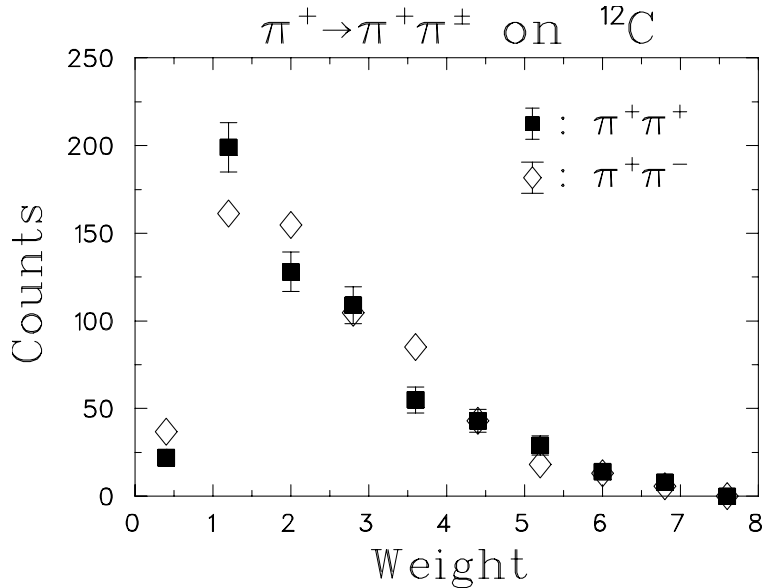


Figure 4: Weight distributions for reconstructed $\pi^+ \rightarrow \pi^+ \pi^\pm$ events on ^{12}C .

invariant mass interval where the yields of the $M_{\pi\pi}$ distributions are different from zero (see Fig. 9). The weight distributions appear rather similar and flat, especially over the shorter interval from 280 MeV to 395 MeV, where the $M_{\pi^+\pi^\pm}^C$ yields are not negligible. The flatness of the weight distributions implies that the shape of the measured $M_{\pi^+\pi^\pm}^C$ distributions changes only moderately when corrected for the CHAOS acceptance. The same conclusion applies to the other nuclei.

The angular and momentum resolutions were measured during the CHAOS commissioning, which just preceded the present measurement. The angular resolution was $< 0.5^\circ$, and the momentum resolution was 1% (σ) for a 1 T magnetic field and 225 MeV/c pions [24]. However, for the pion-production experiment, the pion mean momentum was ≈ 130 MeV/c (see Table 5), and the CHAOS field was set at 0.5 T. Simulations show that under these conditions, the angular resolution, which was dominated by the multiple scattering, is below 2° , and the momentum resolution is $\sim 4\%$ (σ) for 130 MeV/c pions.

2.5 Particle identification

In the case of pion-production studies, pions must be selectively separated from other reaction byproducts, essentially from e, p and d , because the $\pi \rightarrow \pi\pi$ reaction cross section in nuclei is from 2 to 3 orders of magnitude lower than the cross section of other competing reactions. For instance, at $T_{\pi^+} \sim 280$ MeV and for ^{40}Ca , the quasi-elastic scattering process $\pi^+ \rightarrow \pi^+ p$ has a total cross section $\sigma_{qes} \sim 800\sigma_{\pi^+\pi^+}$, while the pion absorption process

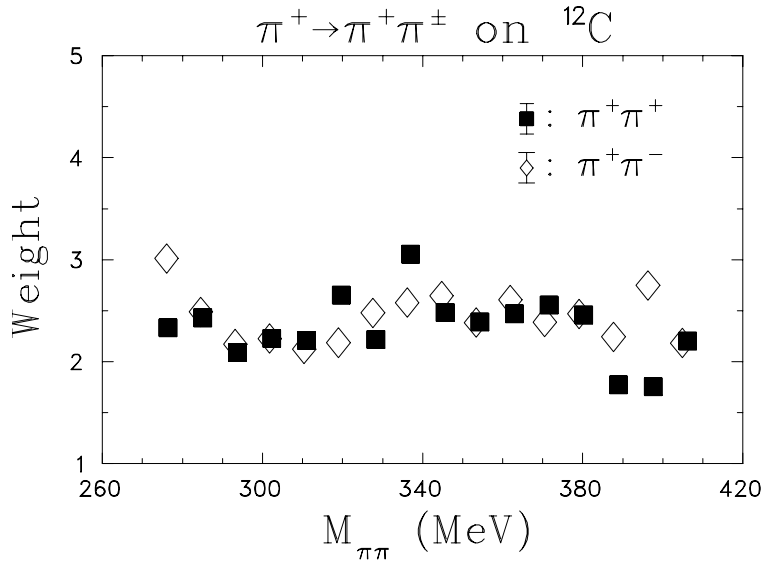


Figure 5: Weight distributions used to correct the $\pi\pi$ invariant mass for the $\pi^+ \rightarrow \pi^+\pi^\pm$ reaction channels on ^{12}C . For a direct comparison, the $M_{\pi\pi}$ scale in the present figure is the same as the scale used in Fig. 9.

$\pi^+ \rightarrow pp$ has a total cross section $\sigma_{abs} \sim 600\sigma_{\pi^+\pi^+}$. For other processes like single charge exchange (scx) $\pi^+ \rightarrow \pi^0$, the background arises from the $\pi^0 \rightarrow \gamma\gamma$ decay followed by the γ conversion $\gamma \rightarrow e^+e^-$ in the target or in the material which surrounds the target. In this case the e^+e^- pair may emulate a $\pi^+\pi^-$ pair.

Particles were identified by combining the information provided by WC's (particle momentum and polarity) and CFT's (pulse heights). For reactions with protons (deuterons) in the final state, i.e. qes and abs, the particle separation was easily achieved through the different response function of $\Delta E1$ and $\Delta E2$ to π 's and p's (d's). Pions from the pion-production process have a momentum distribution which does not exceed 210 MeV/c (see Fig. 14). At this momentum, $PH_p/PH_\pi \sim 6$, and increases as the momentum decreases, see Fig. 8 in Ref.[26] and Fig. 3 in Ref.[12]. However, the same method of particle separation could not successfully be applied to π 's and e's for momenta exceeding 140 MeV/c. Thus, Cerenkov counters were used. These counters were capable of separating π 's from e's with an efficiency of about 95% for particle momenta up to about 230 MeV/c [26] Fig. 11. This value increased slightly ($\sim 98\%$) when the Cerenkov pulse heights were combined with the $\Delta E1$ and $\Delta E2$ pulse heights. Finally, the π to p and e discrimination turned out to be $\sim 100\%$ when the following soft kinematic cuts were applied to particle momenta and angles:

- Protons which passed the pion PH test were definitively rejected by restricting their momenta below 210 MeV/c, the maximum momentum available to pions. Such a momentum was slightly above the CHAOS threshold to protons, 185 MeV/c.

Table 3: Number of $\pi^+ \rightarrow \pi^+\pi^\pm$ reconstructed events used in the present analysis.

Nucleus	Number of events [$\times 10^3$]	
	$\pi^+ \rightarrow \pi^+\pi^-$	$\pi^+ \rightarrow \pi^+\pi^+$
2H	7.27	1.06
^{12}C	6.89	0.62
^{40}Ca	4.94	0.49
^{208}Pb	3.69	0.31

- Electron pairs, which might emulate $\pi^+\pi^-$ pairs, appeared with opening angles $< 2^\circ$. This is in accord with simulations of the $\pi^0 \rightarrow \gamma\gamma$ decay followed by the γ conversion $\gamma \rightarrow e^+e^-$ in CHAOS. Therefore a 2° cut was applied during the analysis, which resulted in a $\sim 0.3\%$ reduction of the $\pi^2\pi$ in-the-reaction plane phase space.

3. Analysis

The data reduction was based on fully reconstructed $\pi^+ \rightarrow \pi^+\pi^-$ and $\pi^+ \rightarrow \pi^+\pi^+$ events. Table 3 reports the yields for each channel and nucleus studied. In order to form differential cross sections these events were binned with their weights, which include the $\pi^+\pi^\pm$ decay rates inside CHAOS. Some particularly useful distributions are represented included those of the canonical observables such as invariant mass $M_{\pi\pi}$, angles Θ_π , $\Theta_{\pi\pi}$, $\cos\Theta_{\pi\pi}^{CM}$, and kinetic energy T_π .

The ability to measure the kinetic energies (T) and laboratory angles (Θ) of both final state pions with the CHAOS spectrometer permitted the determination of the five-fold differential cross section $\partial^5\sigma/(\partial T\partial\Theta)_{\pi_1}(\partial T\partial\Theta)_{\pi_2}\partial\Phi_{\pi_1\pi_2}$. Here, $\Phi_{\pi_1\pi_2}$ is the zenithal angle between π_1 and π_2 , which, in the CHAOS detector, can be measured at either $180^\circ \pm 7^\circ$, or $0^\circ \pm 7^\circ$. Four-fold differential cross sections were then obtained by integrating out the $\Phi_{\pi\pi}$ dependence. This was accomplished by using a linear function joining the two measured data points, and the result was the factor f_Φ . This method of assessing f_Φ leads to a systematic uncertainty of 8% (σ) for deuterium [8] and 6-7% (σ) for nuclei. The data were also reduced to single differential cross sections $d\sigma/d\mathcal{O}_\pi$, where \mathcal{O}_π represents (T_π or Θ_π)_{1,2}. The cross section was then related to measured quantities $\frac{d\sigma}{d\mathcal{O}_\pi} = f_e \frac{N(\mathcal{O}_\pi)}{\Delta\mathcal{O}_\pi}$, where f_e is a parameter which is determined by the experimental conditions, $N(\mathcal{O}_\pi)$ is the number of weighted events in a given bin and $\Delta\mathcal{O}_\pi$ is the bin width for the \mathcal{O}_π observable. The experimental parameter f_e is the product of several factors which were individually measured in order to obtain absolute values for the cross sections: $f_e = f_\Phi(N_\pi\mathcal{C}_l\mathcal{E}_{WC}N_{sc})^{-1}$, where N_π is the number of pions impinging upon the target (see discussion in Paragraph 2.1), \mathcal{C}_l is the computer live-time during

data acquisition which was 61% for 2H , 53% for ${}^{12}C$, 70% for ${}^{40}Ca$ and 80% for ${}^{208}Pb$, \mathcal{E}_{WC} is the overall WC efficiency 49.5%, and N_{sc} is the number of target scattering centres per unit area (see discussion in Paragraph 2.2). The uncertainty in $f_e \sim 11\%$ (σ) comes mostly from the uncertainties in \mathcal{E}_{WC} and f_Φ . In fact, $\mathcal{E}_{WC} = \mathcal{E}_{WC1}\mathcal{E}_{WC2}(\mathcal{E}_{WC1}\mathcal{E}_{WC2}\mathcal{E}_{WC3})^2$, and the average uncertainty in measuring the efficiency of a wire chamber was 0.93% thus yielding an overall \mathcal{E}_{WC} uncertainty of 8.3%. The WC4 efficiency uncertainty was 0.0% since only three out of eight independent anodes of one cell were required to fire in order to determine the direction of an outgoing pion. Finally, the overall uncertainty was obtained by summing the uncertainty due to f_Φ and \mathcal{E}_{WC} in quadrature.

4. Models of the $\pi 2\pi$ reaction and the $\pi\pi$ interaction in the nuclear medium

This experiment employed the $\pi^+A \rightarrow \pi^+\pi^\pm A'$ reaction ($\pi 2\pi$) to study the near-threshold $\pi\pi$ interaction as a function of the (average) nuclear density. Other reactions can, in principle, be used for similar studies, eg. the $p \rightarrow \pi\pi$ and $\gamma \rightarrow \pi\pi$ reactions. For any reaction and for a reliable interpretation of the $\pi\pi$ dynamics in nuclear matter, theoretical models should account for both the reaction mechanism, and nuclear distortions (i.e. pion absorption and others). In the case of $\pi 2\pi$, this approach was followed in the work of Refs. [16, 18], which also included the kinematical limits of the experimental apparatus. For those theoretical works which addressed only the dynamics of a $(\pi\pi)_{I=J=0}$ interacting system in nuclear matter, it was useful to define the observable $\mathcal{C}_{\pi\pi}^A$ (see Paragraph 5.5) since it is only weakly dependent on the reaction mechanism and nuclear distortions [13].

Before discussing the data and the comparison with the available theoretical calculations for both the $\pi 2\pi$ reaction and the behaviour of a $\pi\pi$ interacting system in nuclear matter, some details of the models are presented below.

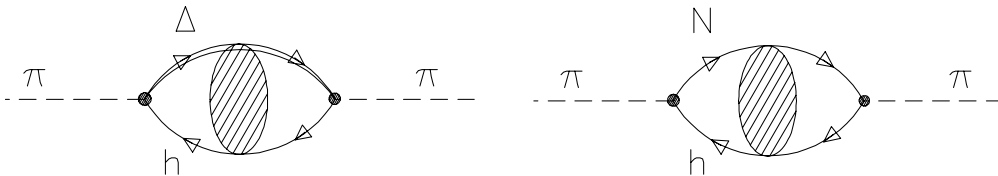


Figure 6: Diagrams depicting the P-wave coupling of pions to $p-h$ and $\Delta-h$ correlated states.

M1: In order to understand the main features of medium modification on the $\pi\pi$ interacting system [18], the pion-production reaction on nuclei is modelled by means of the two leading reactions: 1) the one-pion exchange (OPE) reaction, $\pi^+N \rightarrow \pi^+\pi^\pm N$, which contributes to both the isoscalar and isotensor channels, and 2) the $N^*(1440)$ resonance

excitation which is restricted to decay only to isoscalar $\pi\pi$ states, $\pi^+N \rightarrow N^* \rightarrow \epsilon N \rightarrow N(\pi\pi)_{I=J=0}$. The in-vacuum $\pi\pi$ interaction is accounted for by the chirally-improved Jülich model[29], which in the GeV region is able to describe the $\pi\pi \rightarrow \pi\pi$ scattering and to reproduce the $I = J = 0$ $\pi\pi$ phase shifts. The S -wave $\pi\pi$ (final state) interaction is modified in the nuclear medium through standard renormalization of the pion propagator (see Fig. 6) which determines the following: in the $\pi^+\pi^-$ channel, the isoscalar $\pi\pi$ amplitude is strongly reshaped which finally provides the near-threshold $M_{\pi^+\pi^-}$ enhancement observed in the CHAOS data; in the $\pi^+\pi^+$ channel, the nuclear density has little effect on the pure isotensor $\pi\pi$ amplitude. In order to have a realistic comparison with the CHAOS results, the model deals with common nuclear effects like Fermi motion and pion absorption although using approximate approaches, and calculates the many-fold differential cross sections by accounting for the CHAOS acceptance.

M2: The effort in Ref.[16] is to model the $\pi^+A \rightarrow \pi^+\pi^\pm A'$ reaction through a microscopic description of the elementary $\pi N \rightarrow \pi\pi N$ reaction and a detailed study of the production reaction in nuclei. The elementary pion-production reaction relies on five

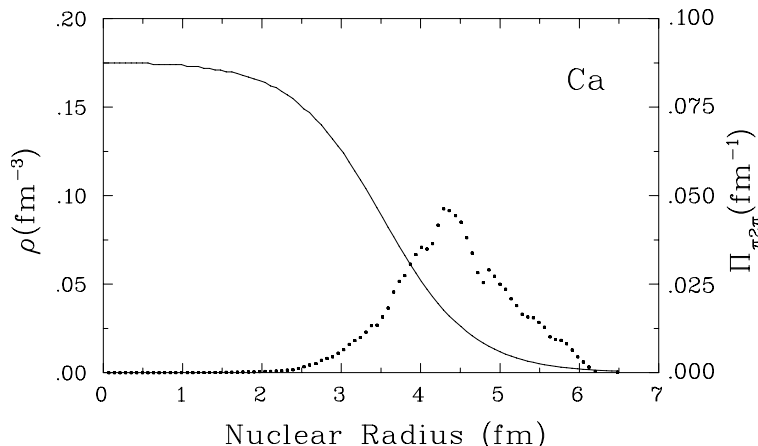


Figure 7: Nuclear density distribution (ρ , solid curve) and probability of a $\pi^2\pi$ event to occur ($\Pi_{\pi^2\pi}$, dotted curve) for Ca as a function of the nuclear radius. The area subtended by $\Pi_{\pi^2\pi}$ is normalized to 1.

Feynmann diagrams, which have N 's, Δ 's and N^* 's as intermediate isobars. The relative scattering amplitudes are derived from chiral lagrangian. The purely mesonic $\pi\pi$ amplitude is calculated by means of the coupled-channel Bethe-Salpeter equation, and the resulting amplitude is capable of predicting the experimental phase shifts of the scalar-isoscalar channel up to 1.2 GeV. With this detailed approach to the $\pi N \rightarrow \pi\pi N$ reaction, the model is able to predict the total cross sections for the $\pi^+\pi^-$, $\pi^0\pi^0$ and $\pi^+\pi^+$ channels from threshold up to 300 MeV. In the nuclear medium, the $(\pi\pi)_{I=J=0}$ interaction is strongly modified due to the coupling of pions to $p-h$ and $\Delta-h$ excitations, which are represented by the diagrams in Fig. 6. This results in a displacement

of the $ImT_{\pi\pi}$ strength toward the $2m_\pi$ threshold as the nuclear density increases. Conversely, the nuclear medium weakly affects the $(\pi\pi)_{I=2, J=0}$ interaction.

The model includes several nuclear effects: Fermi motion, Pauli blocking, pion absorption and quasi-elastic scattering. The last two interactions are found to largely remove $\pi 2\pi$ pions from the incident flux, which ultimately confines the pion-production process on the nuclear skin[30]. Fig. 7 shows the probability of a $\pi 2\pi$ event to occur ($\Pi_{\pi 2\pi}$, dotted curve) along with the nuclear density distribution (ρ , solid curve) for Ca as a function of the nuclear radius. The two distributions yield a weighted mean nuclear density of $\rho = 0.24\rho_n$, which qualitatively agrees with the experimental result reported in[12], where the interacting nucleon of the $\pi N[A-1] \rightarrow \pi\pi N[A'-1]$ reaction is found to preferentially lie in an external nuclear orbit. The above value of ρ can also be used for comparison with the nuclear densities quoted in Ref.[18] and discussed in the Paragraph 5.1. Finally, the model employs a Monte Carlo technique to generate and propagate $\pi 2\pi$ events, thus their phase space can easily accommodate the CHAOS acceptance.

- M3:** The work of Ref.[17] aims at studying the possibility of the σ -meson identification in nuclear matter, where the elusive particle might be detected as a consequence of the partial restoration of chiral symmetry. Due to the strong interaction of σ with the nuclear medium, the description of the σ properties in terms of parameters like m_σ and Γ_σ appears inadequate, and a proper observable becomes the σ spectral function ρ_σ . By using a simple but general approach, [17] proves that in the proximity of the $2m_\pi$ threshold the partial restoration of the chiral symmetry implies $\rho_\sigma(\omega \sim 2m_\pi) = -\pi^{-1}/Im\Sigma_\sigma(\omega, \rho)$, where Σ_σ is the σ self-energy, ω is the total energy and ρ the nuclear density. Near $2m_\pi$ threshold, the $Im\Sigma_\sigma$ is proportional to the phase space factor $(1 - \frac{2m_\pi^2}{\omega^2})^{1/2}$, thus $\rho_\sigma(\omega \sim 2m_\pi) \propto \theta(\omega - 2m_\pi)/(1 - \frac{2m_\pi^2}{\omega^2})^{1/2}$. A direct consequence is that the σ spectral function strength enhances as the σ total energy approaches $2m_\pi$. In order to render this general finding more quantitative, the theory uses the SU(2) linear sigma model. The mean field correction in nuclear matter of $\Sigma_\sigma(\rho)$ is accounted for by the leading diagram sketched in Fig. 8. Furthermore, the model does not include collective pionic modes to derive a possible source of near-threshold strength from the pion coupling to $p-h$ and $\Delta-h$ correlated states.
- M4:** This work[19] studies the $(\pi\pi)_{I=J=0}$ interaction in nuclear matter by constructing a microscopic theory for both the σ -meson propagator (D_σ) and the $\pi\pi T$ -matrices in the framework of the linear sigma model. In this approach the basic chiral symmetry constraints, i.e. the vanishing of the scattering length in the chiral limit and the Ward's identities are satisfied, and in addition, the theory is capable of reproducing the experimental phase shift in the scalar-isoscalar channel. In-medium pions are renormalized through their P -wave coupling to correlated $p-h$ and $\Delta-h$ states, as depicted in Fig. 6. Bare sigmas, of the linear sigma model, are coupled to the nuclear medium via the tad-pole diagram, which is sketched in Fig. 8. The P -wave renormalization of sigmas leads to a downward shifts of the σ mass, which ultimately produces a strong enhancement of the σ -meson mass distribution (i.e. ImD_σ) around

the $2m_\pi$ threshold. This enhancement is further increased by a factor of 2 to 3 by the S -wave renormalization of the bare σ -meson mass (i.e. by the partial restoration of chiral symmetry), which presents a similar behavior near the $2m_\pi$ threshold.

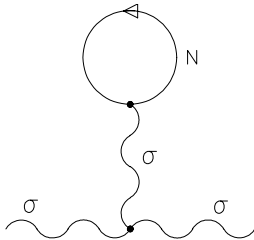


Figure 8: Diagram (tad-pole) describing the S -wave coupling of σ to the nuclear medium.

5. Results of the $\pi \rightarrow \pi\pi$ reaction in nuclei

A general property of the $\pi 2\pi$ process on nuclei in the low-energy $M_{\pi\pi}$ regime was outlined by previous experimental works: it is a quasi-free process both when it occurs on deuterium [28] and on complex nuclei [12]. Furthermore, a common reaction mechanism underlies the process whether it occurs on a nucleon or a nucleus [13]. Thus the study of the $\pi^+ {}^2H \rightarrow \pi^+\pi^\pm NN$ reaction is dynamically equivalent to studying the elementary $\pi^+n \rightarrow \pi^+\pi^-p$ and $\pi^+p \rightarrow \pi^+\pi^+n$ reactions separately.

In the present measurement, the $\pi^+A \rightarrow \pi^+\pi^\pm A'$ reactions were studied under the same experimental conditions. Thus for a given observable the distributions are directly comparable. The error bars explicitly shown on the spectra represent the statistical uncertainties, which must be added in quadrature to the systematic one $\sim 11\%$ (σ) to obtain the overall uncertainty associated with the data points. The only exception is for the $\cos\Theta_{\pi\pi}$ distributions in Fig. 10, where the overall uncertainties are shown.

5.1 The $\pi\pi$ invariant mass

Fig. 9 shows the single differential cross sections (diamonds) as a function of the $\pi\pi$ invariant mass ($M_{\pi\pi}$, MeV) for the two reaction channels $\pi^+ \rightarrow \pi^+\pi^-$ and $\pi^+ \rightarrow \pi^+\pi^+$. Horizontal error bars are not indicated since they lie within symbols. The distributions span the total energy interval available to the $\pi 2\pi$ reaction, which ranges from $2m_\pi$, the low-energy threshold, up the 420 MeV, the maximum allowed by the reaction. The $\pi A \rightarrow \pi\pi N[A-1]$ phase space simulations (dotted histograms for $A : {}^2H, {}^{12}C, {}^{40}Ca$ and ${}^{208}Pb$) are also shown, and are normalized to the same area as the experimental distributions.

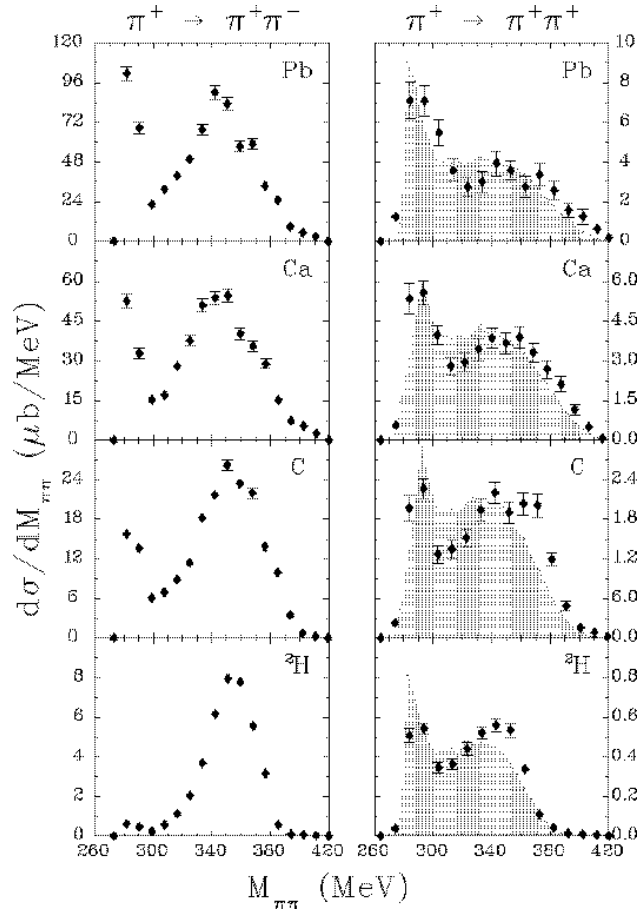


Figure 9: Invariant mass distributions (diamonds) for the $\pi^+ \rightarrow \pi^+\pi^-$ and $\pi^+ \rightarrow \pi^+\pi^+$ reactions on ${}^2\text{H}$, ${}^{12}\text{C}$, ${}^{40}\text{Ca}$ and ${}^{208}\text{Pb}$. The shaded regions represent the results of phase-space simulations for the pion-production reaction $\pi A \rightarrow \pi\pi N[A-1]$.

Regardless of the nuclear mass number, the invariant mass distributions for the $\pi^+ \rightarrow \pi^+\pi^+$ channel closely follow phase space, and the energy maximum increases with increasing A , that is, with increasing nuclear Fermi momentum. The $\pi^+ \rightarrow \pi^+\pi^-$ channel displays a different behaviour. Compared to phase space, the ${}^2\text{H}$ invariant mass displays little strength from $2m_\pi$ to 310 MeV, while, in the same energy interval, the ${}^{12}\text{C}$, ${}^{40}\text{Ca}$ and ${}^{208}\text{Pb}$ $\pi^+\pi^-$ invariant mass distributions increasingly peak as A increases.

In order to explain the nature of the reaction mechanism contributing to the peak structure, it is useful to examine $\cos\Theta_{\pi\pi}^{CM}$ distributions and (p_{π^+}, p_{π^-}) diffusion plots for those events with invariant masses in the region of the peak. $\Theta_{\pi\pi}^{CM}$ is the angle between the direction of a final pion and the direction of the incoming pion beam in the $\pi^+\pi^-$ rest frame. Fig. 10 shows the $\cos\Theta_{\pi\pi}^{CM}$ distributions (diamonds) for $2m_\pi \leq M_{\pi^+\pi^-} \leq 310$ MeV and $310 < M_{\pi^+\pi^-} \leq 420$ MeV, the latter being shown for comparison. The vertical error bars

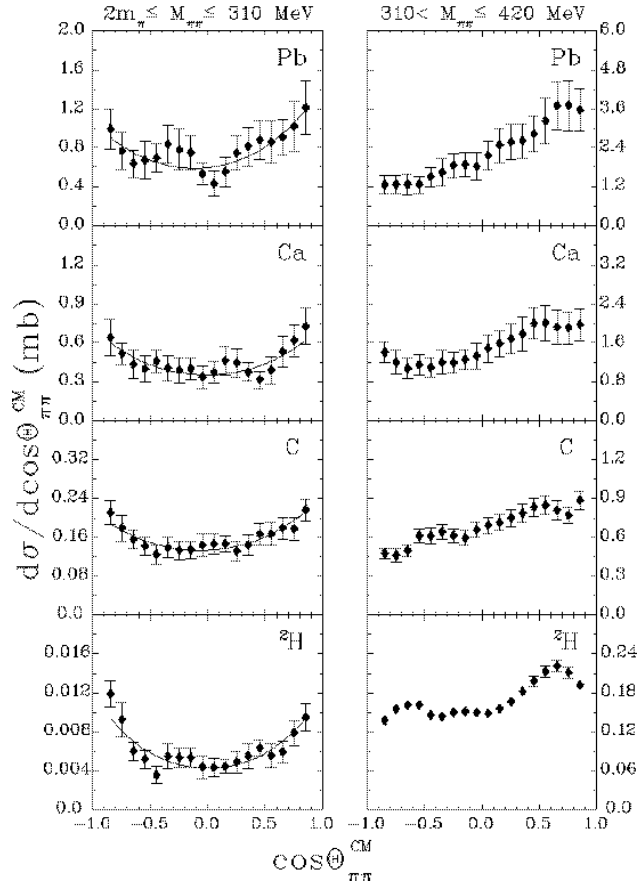


Figure 10: Distribution of $\cos\Theta$ in the $\pi^+\pi^-$ centre-of-mass frame for the $\pi^+A \rightarrow \pi^+\pi^-A'$ reaction for $2m_\pi \leq M_{\pi\pi} \leq 310$ MeV (left frame), and for $310 < M_{\pi\pi} \leq 420$ MeV (right frame). The solid lines are best-fits to the data including S, P and D waves.

represent the overall uncertainties, which are the systematic and statistical uncertainties summed in quadrature. The solid lines in Fig. 10 represent the best-fit to the differential distributions, which was obtained with a partial wave expansion limited to the three lowest waves, i.e. S, P and D. The best-fit results are reported in Table 4, along with χ_ν^2 , which was evaluated using the overall uncertainties. For all the nuclei studied $\chi_\nu^2 \leq 1$ which indicates that a proper number of waves was used in the expansion. In the case of heavier nuclei, the $\pi^+\pi^-$ system predominantly couples in S -wave $\sim 95\%$ (or $\ell=0$ relative angular momentum) and a remaining 5% is spent in a D -wave ($\ell=2$) state. Furthermore, within the sensitivity of the χ_ν^2 -method, any P -wave ($\ell=1$) coupling of the two pions is excluded. Fig. 11 displays the diffusion plots of final pion momenta for the $\pi^+ \rightarrow \pi^+\pi^-$ reaction channel. For the plots on the left side, $M_{\pi^+\pi^-}$ is constrained to the peak region, i.e. $2m_\pi \leq M_{\pi\pi} \leq 310$ MeV. The plots on right side, reported for comparison, are for invariant masses in the higher energy region, $310 < M_{\pi\pi} \leq 420$ MeV. In the peak region, 2H has the pion momenta flatly diffused over the available phase space, while for the more complex nuclei, the choice of $M_{\pi^+\pi^-} \leq 310$ MeV highlights a bump structure in the momentum range 90-140 MeV/c. Generally, the

Table 4: S - P - and D -wave contributions to the $\pi^+ \rightarrow \pi^+\pi^-$ reaction channel for $2m_\pi \leq M_{\pi^+\pi^-} \leq 310$ MeV.

Nucleus	S -wave (%)	P -wave (%)	D -wave (%)	χ_ν^2
2H	88.2	0.0	11.8	1.03
${}^{12}C$	96.0	0.0	4.0	0.29
${}^{40}Ca$	93.9	0.0	6.1	0.43
${}^{208}Pb$	93.9	0.8	5.3	0.46

(p_{π^+}, p_{π^-}) diffusion plots on the right side have a peak-structure which is somewhat wider and centered at higher pion momenta.

The results of two recent theoretical works, $\mathcal{M}1$ [18] and $\mathcal{M}2$ [16], which have modelled the $\pi 2\pi$ reaction on nuclei, are reported in Fig. 12. The (short and long) dashed lines denote the $\mathcal{M}1$ calculations while the $\mathcal{M}2$ predictions are shown as full lines. In the case of Ca , $R1$ ($R2$) indicates the $\mathcal{M}1$ predictions for $\rho=0.7\rho_n$ ($\rho=0.5\rho_n$), where ρ_n is the nuclear saturation density, while $V1$ is the result of the $\mathcal{M}2$ calculations for a mean $\rho=0.24\rho_n$. For the purpose of the present discussion, the curves in Fig. 12 are normalized to the experimental data.

For the $\pi^+ \rightarrow \pi^+\pi^+$ channel, the $R1$ and $R2$ distributions differ slightly from each other. The $R1$ distribution is broader, due to the larger nuclear Fermi momentum, which is a consequence of the higher nuclear density used [18]. The lower ρ used for $R1$ seems to describe the measured distribution better. This trend is also supported by $V1$ whose $\mathcal{M}2$ predictions agree well with the invariant mass distributions. Therefore, both $\mathcal{M}1$ and $\mathcal{M}2$ indicate that the average nuclear density of ${}^{40}Ca$ for which the production reaction takes place cannot exceed $0.5\rho_n$.

In the $\pi^+ \rightarrow \pi^+\pi^-$ channel the distribution predicted by $\mathcal{M}2$ for 2H is able to describe the data, although it tends to overestimate the low-energy $M_{\pi\pi}$ yield. The present version of the model is considerably improved compared to previous versions [4, 8], thus placing the construction of nuclear medium effects on more reliable grounds. The $\mathcal{M}2$ approach to ${}^{40}Ca$ includes several medium effects: Fermi motion, pion absorption, pion quasi-elastic scattering, and $(\pi\pi)_{I=J=0}$ medium modifications. Nevertheless, the model is unable to reproduce the observed $M_{\pi\pi}$ strength in the near threshold region. An increase of ρ from $0.24\rho_n$ to $0.5\rho_n$ and to $0.7\rho_n$ is unlikely to improve the agreement with the experimental cross section, see also Fig. 9 of Ref.[16]. In the case of $\mathcal{M}1$, the $R2$ prediction ($0.5\rho_n$) seems to reproduce the $M_{\pi\pi}$ distribution better, although some of the near-threshold yield already comes from the $\pi^+ {}^2H \rightarrow \pi^+\pi^- pp$ production. The model, in fact, overestimates the cross section at low invariant masses whose amount is shown in Fig. 12. The $R1$ solution ($0.7\rho_n$) provides the correct $M_{\pi\pi}$ near-threshold intensity but does not describe the remaining part of the distribution very well. Therefore, $V1$, $R1$ and $R2$ suggest that the missing $M_{\pi^+\pi^-}$ strength

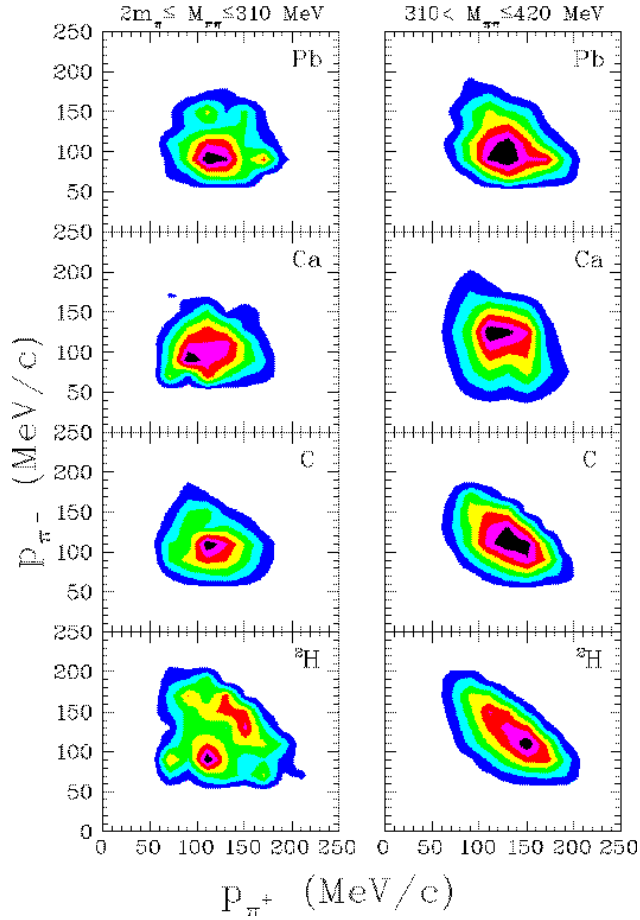


Figure 11: Diffusion plots of final pion momenta for the $\pi^+ \rightarrow \pi^+\pi^-$ reaction channel. The $\pi^+\pi^-$ invariant mass is limited to the peak region $2m_\pi \leq M_{\pi\pi} \leq 310$ MeV (left frame), and to the region above it $310 < M_{\pi\pi} \leq 420$ MeV (right frame).

near the $2m_\pi$ threshold should be searched for in a stronger ρ -dependence of the $(\pi\pi)_{I=J=0}$ interaction, rather than by requiring the pion-production process to occur in an unlikely high-density nuclear environment.

5.2 The $\pi\pi$ opening angle

For the $\pi A \rightarrow \pi_1\pi_2 A'$ production reaction, the relation between the $\pi_1\pi_2$ invariant mass and the directly measured quantities is: $M_{\pi_1\pi_2}^2 = 4m_\pi^2 + 2T_{\pi_1}T_{\pi_2} + 2m_\pi(T_{\pi_1} + T_{\pi_2}) - p_{\pi_1}p_{\pi_2}\cos\Theta_{\pi_1\pi_2}$, where $T_\pi(p_\pi)$ is the pion kinetic energy (momentum) and $\Theta_{\pi_1\pi_2}$ is the opening angle of the pion pair. The behaviour of $\Theta_{\pi_1\pi_2}$ as a function of $M_{\pi_1\pi_2}$ is studied by directly applying soft-cuts on $M_{\pi_1\pi_2}$. Fig. 13 illustrates the differential cross section as a function of $\Theta_{\pi\pi}$ for $2m_\pi \leq M_{\pi\pi} \leq 310$ MeV (crosses), and $2m_\pi \leq M_{\pi\pi} \leq 420$ MeV (diamonds). The differential cross sections nearly coincide for all nuclei from 0° up to 60° , which indicates that

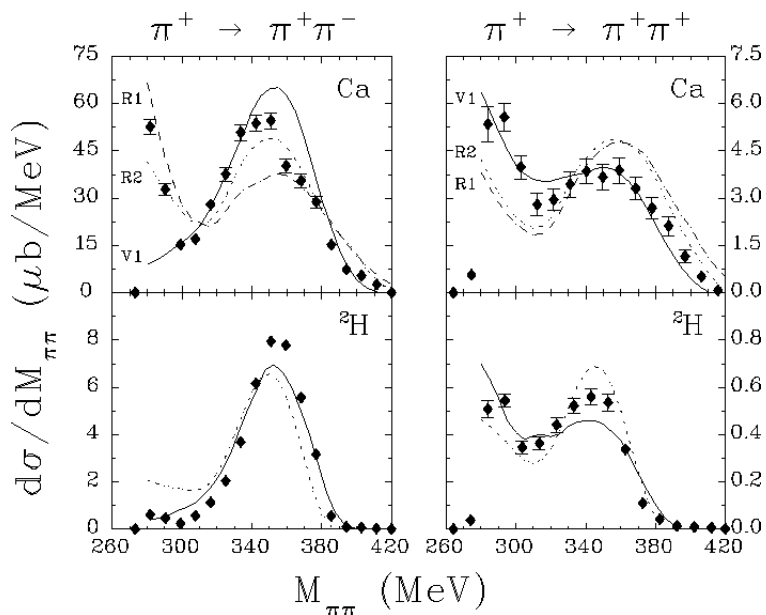


Figure 12: Invariant mass distributions (diamonds) for the $\pi^+ \rightarrow \pi^+\pi^-$ and $\pi^+ \rightarrow \pi^+\pi^+$ reactions on ${}^2\text{H}$ and ${}^{40}\text{Ca}$. The dashed curves are taken from Ref.[18] and the model is explained in $\mathcal{M}1$, $R1$ and $R2$ are the results for $0.7\rho_n$ and $0.5\rho_n$, respectively. The full curves ($V1$) are from the theoretical work of Ref.[16] $\mathcal{M}2$ with a mean $\rho=0.24\rho_n$. The curves are normalized to the experimental data.

the near-threshold pion pairs are preferentially emitted at small opening angles, regardless of both the pion energy and the reaction channel. In general, the $\Theta_{\pi\pi}$ distributions for the two reaction channels vary markedly with A , making this observable suitable for selective tests of various $\pi 2\pi$ models.

5.3 The π energy

Table 5: Centroids (in MeV) of the single pion kinetic energy distributions for the $\pi^+ \rightarrow \pi^+\pi^-$ channel (\mathcal{C}_+ and \mathcal{C}_-) and for the $\pi^+ \rightarrow \pi^+\pi^+$ channel (\mathcal{C}_+). The uncertainties (σ) in evaluating \mathcal{C} 's are reported in parenthesis.

Nucleus	$\pi^+ \rightarrow \pi^+\pi^-$		$\pi^+ \rightarrow \pi^+\pi^+$
	\mathcal{C}_+	\mathcal{C}_-	\mathcal{C}_+
${}^2\text{H}$	50.7(0.4)	45.5(0.4)	52.5(0.5)
${}^{12}\text{C}$	47.5(0.4)	40.8(0.4)	48.4(0.5)
${}^{40}\text{Ca}$	48.9(0.5)	38.6(0.5)	49.4(0.6)
${}^{208}\text{Pb}$	50.7(0.5)	37.2(0.5)	49.3(0.7)

Fig. 14 shows the differential cross sections for the two $\pi^+A \rightarrow \pi^+\pi^\pm A'$ reactions as a function of the kinetic energy of each final pion. The weighted averages of the distributions

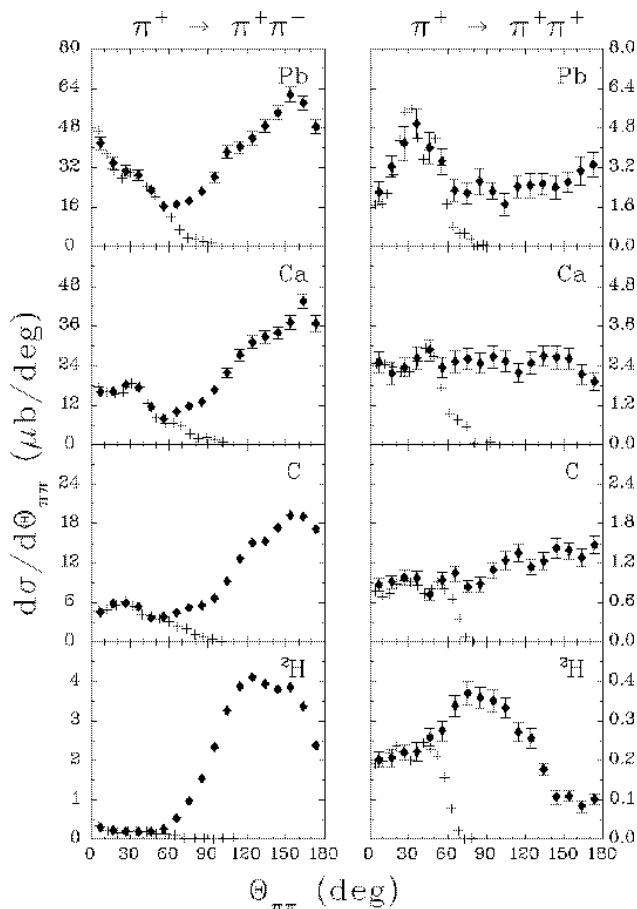


Figure 13: Opening angle distributions for the $\pi^+ \rightarrow \pi^+\pi^-$ and $\pi^+ \rightarrow \pi^+\pi^+$ reactions on ${}^2\text{H}$, ${}^{12}\text{C}$, ${}^{40}\text{Ca}$ and ${}^{208}\text{Pb}$ for $2m_\pi \leq M_{\pi\pi} \leq 310$ MeV (crosses) and for $2m_\pi \leq M_{\pi\pi} \leq 420$ MeV (diamonds).

are reported in Table 5. \mathcal{C}_+ and \mathcal{C}_- refer to the centroids of the distributions, in MeV, for positive and negative pions, respectively. The \mathcal{C}_+ 's display a weak A -dependence. For the complex nuclei the mean energy is 49.0 ± 1.0 MeV which is similar to the mean energy of 51.6 ± 0.9 MeV for ${}^2\text{H}$. This can be explained by observing that the nuclear Coulomb repulsion on final pions is in part compensated by the same repulsion on initial pions. In the $\pi^+ \rightarrow \pi^+\pi^-$ channel, centroids follow a Coulomb-like behaviour, although the intensity is smaller than expected. In fact, \mathcal{C}_- decreases by 2.2 MeV from ${}^{12}\text{C}$ to ${}^{40}\text{Ca}$, and by 1.4 MeV from ${}^{40}\text{Ca}$ to ${}^{208}\text{Pb}$, while a semi-classical treatment of the nuclear Coulomb attraction on point-like particles yields a decrease of 2.2 MeV and 4.6 MeV, respectively.

In Fig. 14 the experimental T_π distributions are shown, along with results from $\pi^+A \rightarrow \pi^+\pi^+n[A-1]$ phase space simulations. Except for ${}^2\text{H}$, the experimental distributions are well reproduced by the simulations, especially at higher energies, thus giving confidence in the reliability of the data. The result of the simulations cannot be applied to negative pions,

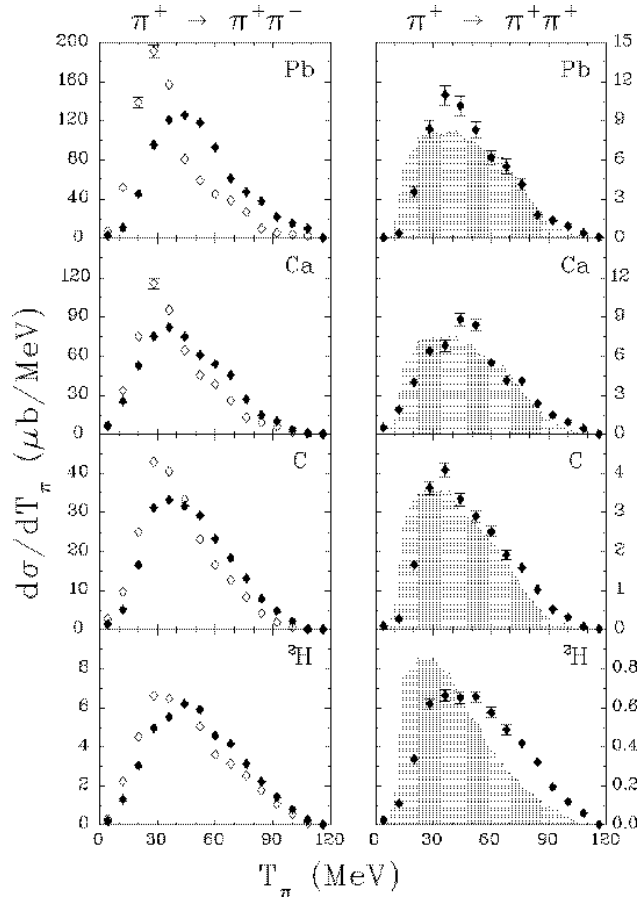


Figure 14: Single pion kinetic energy distributions for the $\pi^+ \rightarrow \pi^+\pi^-$ and $\pi^+ \rightarrow \pi^+\pi^+$ reactions on ${}^2\text{H}$, ${}^{12}\text{C}$, ${}^{40}\text{Ca}$ and ${}^{208}\text{Pb}$. Positive and negative pion distributions are denoted with full and open diamonds, respectively. The shaded areas represent the results of $\pi^+A \rightarrow \pi^+\pi^+n[A-1]$ simulations. The CHAOS threshold for pions is 11 MeV.

since the energy losses of π^- 's due to Coulomb interactions is not exactly known. The kinetic energy distributions are not compared to the results of any theoretical predictions because none are available at this time.

5.4 The π angles

In order to complete the discussion of the canonical observables, in Fig. 15 the $\cos\Theta_\pi$ differential cross sections are reported, where pion angles are in the laboratory frame and $\cos\Theta_\pi=1$ coincides with the direction of the incident pion. Positive and negative pion distributions are denoted with full and open diamonds, respectively. The interpretation of these distributions awaits microscopic $\pi 2\pi$ calculations, since phase space simulations cannot describe the observed bump structures.

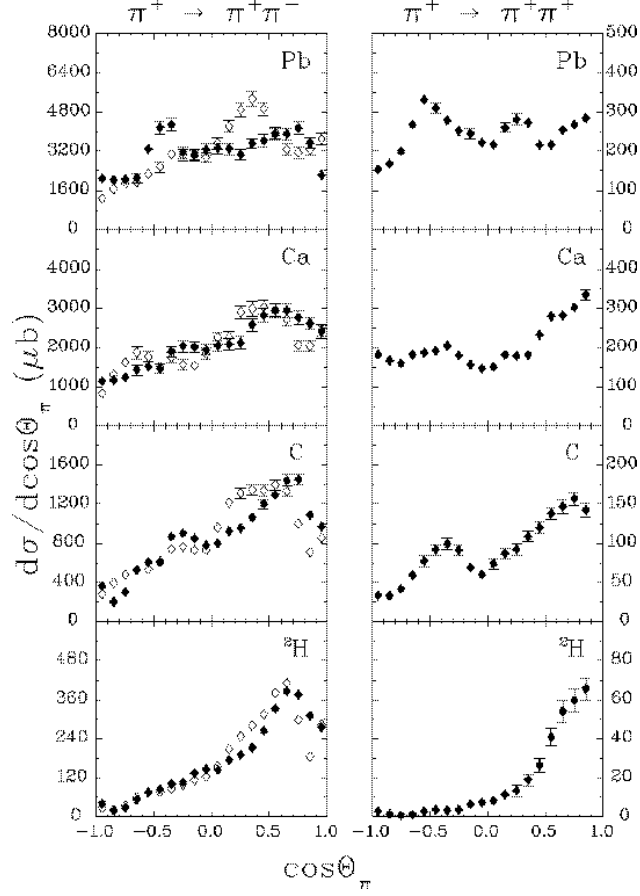


Figure 15: Distributions of $\cos\Theta_\pi$ for the $\pi^+ \rightarrow \pi^+\pi^-$ and $\pi^+ \rightarrow \pi^+\pi^+$ reactions on ${}^2\text{H}$, ${}^{12}\text{C}$, ${}^{40}\text{Ca}$ and ${}^{208}\text{Pb}$. Positive and negative pion angular distributions are in the laboratory frame, and are denoted with full and open diamonds, respectively.

5.5 The $\mathcal{C}_{\pi\pi}^A$ ratio

In this paragraph the observable $\mathcal{C}_{\pi\pi}^A$ is presented in comparison with recent theoretical predictions. $\mathcal{C}_{\pi\pi}^A$ is defined as the composite ratio $\frac{M_{\pi\pi}^A}{\sigma_T^A} / \frac{M_{\pi\pi}^N}{\sigma_T^N}$, where σ_T^A (σ_T^N) is the measured total cross section of the $\pi 2\pi$ process in nuclei (nucleon). This observable has the property of yielding the net effect of nuclear matter on the $(\pi\pi)_{I=J=0}$ interacting system regardless of the $\pi 2\pi$ reaction mechanism used to produce the pion pair [13]. Therefore, $\mathcal{C}_{\pi\pi}^A$ can be compared not only with the $\mathcal{M}1$ and $\mathcal{M}2$ predictions which explicitly calculate both $M_{\pi\pi}^{\text{Ca}}$ and $M_{\pi\pi}^{{}^2\text{H}}$, but also with the theories described in $\mathcal{M}3$ and $\mathcal{M}4$ because they calculate the mass distribution of an interacting $(\pi\pi)_{I=J=0}$ system (i.e. $\text{Im}D_\sigma$) both in vacuum and in nuclear matter. Since the calculations are reported either in arbitrary units [16, 18] or in units which are complex to scale [17, 19], theoretical predictions are normalized to the experimental distributions at $M_{\pi\pi}=350\pm 10$ MeV, where the $\mathcal{C}_{\pi\pi}^A$ distribution is flat.

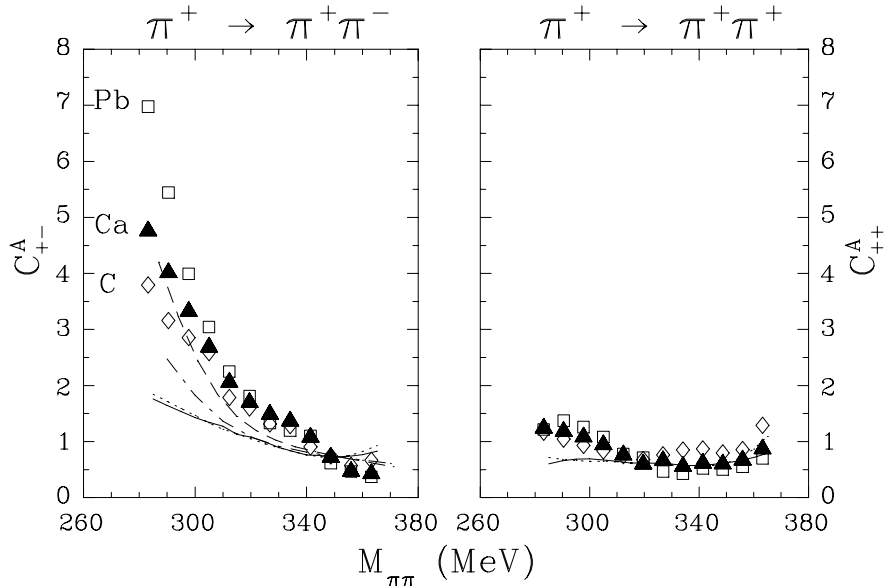


Figure 16: The composite ratios $\mathcal{C}_{\pi\pi}^A$ for ^{12}C , ^{40}Ca and ^{208}Pb . The curves are taken from [16] (full) and the model is described in $\mathcal{M}2$, [17] (dash-dotted) $\mathcal{M}3$, [18] (dotted) $\mathcal{M}1$ and [19] (dashed) $\mathcal{M}4$. Further details are reported in the text.

For both reaction channels, the full[16] and dotted [18] curves in Fig. 16 are obtained by simply dividing $M_{\pi\pi}^{Ca}/M_{\pi\pi}^{2H}$. It is worthwhile recalling that for [18] the option $\rho=0.5\rho_n$ is used while for [16] the mean density is $\rho=0.24\rho_n$. Furthermore, for both approaches the underlying medium effect is the P -wave coupling of π 's to $p-h$ and $\Delta-h$ configurations, which accounts for the near-threshold enhancement. When applied to the $\mathcal{C}_{\pi\pi}^{Ca}$, both $\mathcal{M}1$ and $\mathcal{M}2$ predict the same result, which describes the behaviour of \mathcal{C}_{++}^{Ca} fairly well throughout most of the $M_{\pi\pi}$ energy range, but only reproduces a small part of the near-threshold strength for \mathcal{C}_{+-}^{Ca} .

$\mathcal{M}3$ [17] and $\mathcal{M}4$ [19] examine the medium modifications on the scalar-isoscalar meson, the σ -meson. Nuclear matter is assumed to partially restore chiral symmetry, and consequently m_σ is assumed to vary with ρ . The variation is parametrized as $1 - p\frac{\rho}{\rho_n}$, where p is $0.1 \leq p \leq 0.3$ for $\mathcal{M}3$, and $0.2 \leq p \leq 0.3$ for $\mathcal{M}4$, and for both is $\rho=\rho_n$. Both models are capable of yielding large strength near the $2m_\pi$ threshold, therefore the results for \mathcal{C}_{+-}^A are compared for a common minimum value of the parameter $p=0.2$. In addition, the choice $\rho=\rho_n$ may result appropriate for ^{208}Pb but it is not for medium (i.e. ^{40}Ca) and light (i.e. ^{12}C) nuclei. In Fig. 16 the predictions of $\mathcal{M}3$ and $\mathcal{M}4$ are shown as the dash-dotted curves and dashed curves, respectively. $\mathcal{M}4$ predicts a larger near-threshold strength, which is due to the combined contributions of the in-medium P -wave coupling of pions to $p-h$ and $\Delta-h$ configurations, and to the partial restoration of chiral symmetry in nuclear matter. These two models, however, are still too schematic for a conclusive comparison to the present data, and full theoretical calculations are called for.

6. Existing $\pi 2\pi$ results

Novel $\pi 2\pi$ results [31] were recently presented by the Crystal Ball (CB) Collaboration at the AGS. The $\pi^- A \rightarrow \pi^0 \pi^0 A'$ production reaction was studied on several nuclei H , ^{12}C , ^{27}Al and ^{64}Cu at incident pion momenta (energies) of $p_{\pi^-}=408$ and 750 MeV/c ($T_{\pi^-}=291.6$ and 623.3 MeV). The figures presented in Ref.[31], however, are only for the results obtained at the higher momentum. In the near-threshold region the $\pi^+\pi^-$ and $\pi^0\pi^0$ channels can be directly compared since they share similar dynamical aspects. The $\pi^0\pi^0$ system cannot be in a P -state, and $\pi^+\pi^-$ does not couple to P -waves (see Paragraph 5.1). Also, the scattering amplitudes of the two reaction channels, $\pi^- \rightarrow \pi^0\pi^0$ and $\pi^+ \rightarrow \pi^+\pi^-$, have the two leading isospin amplitudes $T_{3,2}$ and $T_{1,0}$ in common, where the first (second) index is the total isospin (dipion isospin) [16]. The $M_{\pi^0\pi^0}^A/M_{\pi^0\pi^0}^C$ ratio in Ref.[31] has marked similarities to the observable $\mathcal{C}_{\pi^+\pi^-}^A$. Namely, the two ratios are flat at around 400 MeV invariant mass but increase as $M_{\pi\pi}$ approaches the $2m_\pi$ threshold, and, near threshold, both ratios increase as A increases. Unlike the CHAOS data, the invariant mass distributions in [31] show no evidence of a peak at the $2m_\pi$ threshold. However, the CB and CHAOS spectra do share relevant features: they both have meager $M_{\pi\pi}$ strength near threshold for H (2H for CHAOS), and show a dramatic increase of strength with increasing A . As outlined earlier in the present work, the *CHAOS peak* may be attributed to the finite out-of-plane acceptance of the spectrometer, but the pion distributions are relatively unaffected by nuclear distortions because of the low kinetic energies of the two final pions [12, 13]. The mean kinetic energy of the CB π^0 's, however, may exceed 200 MeV, and at this energy pions may undergo large distortions while leaving the nucleus [32]. Pions may be absorbed and the absorption rate depends on both the pion kinetic energy and its initial position inside a nucleus. In addition, pions scatter via the $\pi A \rightarrow \pi' A$ reaction and change direction. This smears out the $\pi^0\pi^0$ opening angle distributions, and ultimately the $M_{\pi^0\pi^0}$ ones (see discussion in Paragraph 5.2). Such distortions are difficult to model since they depend on both the pion energy and the position inside the nucleus. Thus, in order to study $\pi\pi$ medium modifications, it is advisable to deal with low-energy final pions [12, 13].

7. Conclusions

In this article the results of an exclusive measurement of the pion-production $\pi^+ A \rightarrow \pi^+\pi^\pm A'$ reactions on 2H , ^{12}C , ^{40}Ca , and ^{208}Pb , at an incident pion energy $T_{\pi^+}=283$ MeV, were presented. The primary interest was directed to the study of the $\pi\pi$ -dynamics in nuclear matter. The reaction was initially examined on deuterium in order to understand the elementary pion-production mechanism, then on nuclei in order to determine the effects of medium modifications on the $\pi\pi$ -system. Some of latter effects could be obtained by direct comparison of the $\pi 2\pi$ distributions, since the data were taken under the same kinematical conditions. The $\pi\pi$ properties were highlighted by means of $M_{\pi\pi}$, $\cos\Theta_{\pi\pi}^{CM}$, $\Theta_{\pi\pi}$, etc.

differential cross sections as well as the composite $\mathcal{C}_{\pi\pi}^A$ ratios.

$\mathcal{C}_{\pi\pi}^A$ was found to yield the net effect of nuclear matter on the $\pi\pi$ system regardless of the $\pi 2\pi$ reaction mechanism used to produce the pion pair. These distributions display a marked dependence on the charge state of the final pions. (i) The $\mathcal{C}_{\pi^+\pi^-}^A$ distributions peak at the $2m_\pi$ threshold and their yield increases as A increases, thus indicating that pion pairs form a strongly interacting system. Furthermore, the $\pi\pi$ system couples to $I = J = 0$, the σ -meson channel. (ii) In the $\pi^+ \rightarrow \pi^+\pi^+$ channel, the $\mathcal{C}_{\pi\pi}^A$ distributions show little dependence on either A or T , thus indicating that nuclear matter only weakly affects the $(\pi\pi)_{I,J=2,0}$ interaction.

The $\mathcal{C}_{\pi^+\pi^-}^A$ observable was compared with theories which included the $(\pi\pi)_{I=J=0}$ in-medium modifications associated with the partial restoration of chiral symmetry in nuclear matter, and with model calculations which only included standard many-body correlations, i.e. the P -wave coupling of π 's to $p-h$ and $\Delta-h$ configurations. It was found that both mechanisms are necessary to interpret the data, although chiral symmetry restoration yields the larger near-threshold contribution. If this conclusion is correct, the $\pi 2\pi$ CHAOS data would provide an example of a distinct QCD effect in low-energy nuclear physics.

Monte Carlo simulations of the $\pi^+A \rightarrow \pi^+\pi^\pm N[A-1]$ reaction phase space proved useful in the interpretation of some of the $\pi 2\pi$ data. In the case of $M_{\pi^+\pi^+}$, the distribution of $\pi^+\pi^+$ pairs follows phase space. In addition, simulations are able to describe the high-energy part of the distributions, which are sensitive to the nuclear Fermi momentum of the interacting $\pi^+p[A-1] \rightarrow \pi^+\pi^+n[A-1]'$ proton. The same conclusions apply to the T_{π^+} distributions, thus giving confidence in the reliability of the data. For the $M_{\pi^+\pi^-}$ distributions, the $\pi\pi$ dynamics overwhelms the dipion kinematics. Unlike the phase space simulations, the near-threshold $\pi^+\pi^-$ yield is suppressed in the elementary production reaction, $\pi^+{}^2H \rightarrow \pi^+\pi^-pp$ in the present work, while, in the same energy range, medium modifications strongly enhance $M_{\pi^+\pi^-}$. Any interpretation of the shape of the $M_{\pi^+\pi^\pm}^A$ (or $\mathcal{C}_{\pi^+\pi^\pm}^A$) distributions should combine the effects of the restoration of chiral symmetry in nuclear matter, and standard many-body correlations. Such an approach would not require a high-density nuclear medium to obtain strong $\pi\pi$ medium modification in the proximity of the $2m_\pi$ threshold.

The results of the present measurement were compared with results from the Crystal Ball Collaboration at the BNL, which are the only relevant ones available. The two results show remarkable similarities. The difference in shape of the near-threshold $M_{\pi\pi}^A$ distributions can be ascribed to the limited CHAOS acceptance and to nuclear pion distortions in the case of the CB data. Most important, however, is that the exclusive $\pi 2\pi$ CB measurement independently confirms that the nuclear medium strongly influences the $\pi\pi$ interaction in the $I = J = 0$ channel.

The experiment was performed at the TRIUMF Meson Facility by using the CHAOS spectrometer. The experimental method used in a previous measurement at TRIUMF and the results obtained were similar to those discussed in the present article. However, the first-generation equipment employed and the $\pi^+A \rightarrow \pi^+\pi^-A'$ model used to interpret the results were able to disclose only part of the underlying physics.

Acknowledgements

The authors would like to acknowledge the support received from TRIUMF. The present work was made possible by grants from the Istituto Nazionale di Fisica Nucleare (INFN) of Italy, the National Science and Engineering Research Council (NSERC) of Canada, the Australian Research Council. The authors would also like to acknowledge useful discussions with Z. Aouissat, G. Chanfray, T. Hatsuda, E. Oset, R. Rapp, P. Schuck, M. Vicente-Vacas and J. Wambach.

References

- [1] N. Grion *et al.*, Phys. Rev. Lett. **59**, 1080 (1987).
- [2] N. Grion *et al.*, Nucl. Phys. **A492**, 509 (1989).
- [3] P. Camerini, N. Grion, R. Rui and D. Vetterli, Nucl. Phys. **A552**, 451 (1993).
- [4] E. Oset and M. J. Vicente-Vacas, Nucl. Phys. **A454**, 637 (1986). The model was improved to calculate total cross-sections for $N \neq Z$ nuclei (M. Vicente-Vacas, private communication, 1990).
- [5] F. Bonutti, P. Camerini, N. Grion, R. Rui and D. Vetterli and F. M. Rozon, Phys. Rev. **C47**, 863 (1993).
- [6] P. Schuck W. Nörenberg and G. Chanfray, Z. Phys. **A330**, 119 (1988); G. Chanfray, Z. Aouissat, P. Schuck and W. Nörenberg, Phys. Lett. **B256**, 325 (1991);
- [7] Z. Aouissat R. Rapp, G. Chanfray, P. Schuck and J. Wambach, Nucl. Phys. **A581**, 471 (1995);
- [8] F. Bonutti *et al.*, Nucl. Phys. **A638**, 729 (1998).
- [9] M. Kermani *et al.*, Phys. Rev. **C58**, 3419 (1998).
- [10] M. Kermani *et al.*, Phys. Rev. **C58**, 3431 (1998).
- [11] F. Bonutti *et al.*, Phys. Rev. Lett. **77**, 603 (1996).
- [12] F. Bonutti *et al.*, Phys. Rev. **C55**, 2998 (1997).
- [13] F. Bonutti *et al.*, Phys. Rev. **C60**, 018201(1999).
- [14] P. Schuck, Z. Aouissat, F. Bonutti, G. Chanfray, E. Fragiacomio, N. Grion and J. Wambach, 36th International Winter Meeting on Nuclear Physics, Bormio, Jan. 1998.
- [15] H. C. Chiang, E. Oset and M. J. Vicente-Vacas, Nucl Phys. **A644**, 77(1998);
- [16] M. J. Vicente-Vacas and E. Oset, Phys. Rev. **C60**, 064621(1999).
- [17] T. Hatsuda and T. Kunihiro, Phys. Lett. **B185** 304(1987); T. Hatsuda and T. Kunihiro, Phys. Rep. **247** 221(1994); T. Kunihiro, Prog. of Theor. Phys. Suppl. **120** 75(1995); S. Chiku and T. Hatsuda, Phys. Rev. **D57**, 6(1998); T. Hatsuda, T. Kunihiro and H. Shimizu, Phys. Rev. Lett. **82** 2840(1999).
- [18] R. Rapp, J. W. Durso, Z. Aouissat G. Chanfray, O. Krehl, P. Schuck J. Speth and J. Wambach, Phys. Rev. **C59**, R1237 (1999).

- [19] Z. Aouissat G. Chanfray, P. Schuck and J. Wambach, nucl-th/9908076 v2 31 Aug 1999; D. Davesne Y.J. Zhang and G. Chanfray, nucl-th/9909032 15 Sept 1999.
- [20] Yu. A. Batusov, S.A. Bunyatov, N. Dalkhazhav, G. Ionice, E. Losneanu, V. Mihul, V.S. Sidorov, D. Tuvdendorzh and V.A. Yarba, Sov. J. of Nucl. Phys. **9** 221(1969).
- [21] A. Rahav et al., Phys. Rev. Lett. **66** 1279(1991).
- [22] M. M. Pavan, PhD Thesis, University of British Columbia, 1995.
- [23] P. Camerini, N. Grion, R. Rui, G. Sheffer and R. Openshaw, Nucl. Instr. and Meth. in Phys. Res. **A291**, 557(1990).
- [24] G.R. Smith *et al.*, Nucl. Instr. and Meth. in Phys. Res. **A362**, 349 (1995).
- [25] G. J. Hofman, J. T. Brack, P. A. Amaudruz and G. R. Smith Nucl. Instr. and Meth. in Phys. Res. **A325**, 384 (1993);
- [26] F. Bonutti, S. Buttazzoni, P. Camerini, N. Grion and R. Rui, Nucl. Instr. and Meth. in Phys. Res. **A350**, 136 (1994);
- [27] K. J. Raywood, S. J. McFarland, P. A. Amaudruz, G. R. Smith and M. E. Sevier, Nucl. Instr. and Meth. in Phys. Res. **A357**, 296 (1995).
- [28] R. Rui et al., Nucl. Phys. **A517**, 445 (1990), C. W. Bjork et al., Phys. Rev. Lett. **44**, 62 (1980), J. Lichtenstadt et al., Phys. Rev. **C33**, 655 (1986), V. Sossi et al., Nucl. Phys. **A548** 562 (1992).
- [29] R. Rapp, J. W. Durso and J. Wambach, Phys. Rev. **A596**, 436 (1996).
- [30] M. J. Vicente-Vacas, private communication, Jan 2000; and M. J. Vicente-Vacas and E.Oset, nucl-th/0002010 Feb. 2000.
- [31] B. M. K. Nefkens and A. B. Starostin for the Crystal Ball Collaboration, contribution to: Eighth International Symposium on Meson-Nucleon Physics and the Structure of the Nucleon, Zuoz (Switzerland) Aug 15-21, 1999, published by π NNEWSLETTER No. 15 78(1999).
- [32] J. Hüffner and M. Thies, Phys. Rev. **C20**, 273(1979).